# Partitioning of Macromolecules between Two Interconnected Spherical Cavities

**P. Cifra**†

*Polymer Institute, Slovak Academy of Sciences, Dúbravská cesta 9, 84236 Bratislava, Slovakia*

*Received January 24, 2005; Revised Manuscript Received March 8, 2005*

ABSTRACT: Simulations of excluded volume macromolecular chain encased in two interconnected cavities reveal for weak confinement a strong preference for a conformation of macromolecule in one of the two cavities. For a symmetric twin-cavity system, a conformational transition from the single cavity occupation to the conformation bridging the two cavities is observed on increasing confinement of encased chain. For asymmetric system of cavities with weak confinement the partitioning of chain segments between the two cavities is governed by classical partitioning law in which partitioning free energy increases linearly with chain length. On increasing chain length (or stronger confinement), a maximum in this dependence is observed followed by a decrease. This behavior is explained by correlation between increasing confinement and increasing concentration of encased chain. The position of the maximum reflects an increasing hinderance of the macromolecule in the larger of the two cavities and the start of the population of the bridging conformation as observed from the histogram of conformations. The structure of coils in the twin cavity is reflected by typical structure factors $S(q)$ of (1) the free excluded volume coil for the weak confinement, (2) about the Θ coil for the moderate confinement, and (3) of the polymer globule for strongly confined macromolecular chain exhibiting a break in $S(q)$, appearing from the structure of the twin cavity.

## Introduction

Confinement of flexible macromolecules in small pores is underlying effect in many processes such as separation of macromolecules in gel permeation chromatography or gel electrophoresis. Essential feature in macromolecular confinement is a reduction of conformational entropy of chains.[1] Motivation here, however, is inspired more by biological applications such as macromolecular translocation into or across biomembranes.[2] Other examples are phage infection or translocation of proteins across biomembranes. A similar mechanism is the macromolecular transport in drug delivery or biotechnology of gene transfer. Though real systems are complicated by biological factors a simple model of linear chain translocation into or through pores can provide useful insight into basic principles of effects included in multitude of related applications.

Instead of concentrating on the recently studied typical case of macromolecular translocation through the membrane, we focus here on the equilibrium partitioning between two interconnected cavities. Recently, this effect was experimentally tested by visualization of single DNA molecules fully encased in a twin cavity.[3] While this experiment allows for testing partitioning principles on the single macromolecule in well characterized and monodispersed pores, it allows also for the testing of partitioning in the situation where the partitioning principles were challenged by observed deviation from typical partitioning laws. Linear increase of conformation free energy $\Delta A$ vs $N$ was observed only for weak confinement, for stronger confinement a maximum appeared followed by a decrease.[4] This behavior was explained by increased crowding or variable excluded volume.[4−6] Reported in the twin cavity is also a transition of the polymer conformation from single cavity occupation to a bridging conformation for higher crowding in cavities. For an encased chain in the twin cavity, there exists an intimate interplay of confinement and concentration. In contrast, for partitioning into the confinement from a free solution, the concentration effect on partitioning could be studied separately from the effect of geometrical confinement.[7] Here, for the macromolecule encased in the twin cavity, the confinement and concentration are correlated. Recently, theoretical or simulation studies of translocation through the membrane pore have appeared and are focused especially on kinetics of translocation.[8]

As is often the case molecular simulations can bring new light into complex effects mentioned above. With this aim Monte Carlo molecular simulations are performed here. Results up to now are obtained more on ideal chains with no excluded volume. We evaluate partition coefficient $K$ for partitioning between interconnected cavities and also the distribution of conformations to answer a question on the extent of chain bridging of two cavities. We choose here the simulation in continuum. With respect to lattice simulation we can keep constant aperture between the two cavities (while varying the size and distance of cavities) and also avoid lattice artifacts on the surface of spherical cavities. We present probably the first results for variable chain rigidity in translocation, but the focus is here on flexible chains.

The paper is organized as follows: First, the method of simulation of the macromolecule in twin cavity is described. Then for symmetric and asymmetric systems of interconnected cavities a transition between single cavity occupation and bridging conformation on increasing confinement is described using a histogram of conformations or the partition coefficient. The interplay of confinement and concentration is analyzed for the asymmetric system. Finally, the structure factor of the

† E-mail: cifra@savba.sk Telephone: +421-2-5477 7408. Fax: +421-2-5477 5923.

10.1021/ma050147g CCC: $30.25 
Published on Web 04/06/2005

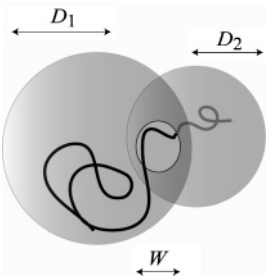


**Figure 1.** Schematic representation of polymer chain encased in interconnected cavities.

chain in the twin cavity is discussed for different confinements.

## Method

For the sake of simulation efficiency and possible contact with other similar studies we use a coarse-grained bead−spring model in which each effective bond in chain is described by finitely extensible nonlinear elastic potential (FENE).[9] Here the bond length varies between $l_{min} = 2l_o - l_{max}$ and $l_{max}$, where $l_o$ is a preferred distance

$$U_{FENE}(l) = -kR^2 \ln\left[1 - \left(\frac{l - l_o}{R}\right)^2\right]$$

$R = l_{max} - l_o$ and $k/k_BT = 20$ is a bond stiffness constant. Typical distances are $l_{min} = 0.4$, $l_o = 0.7$, and $l_{max} = 1$. Most of simulations are performed for fully flexible chains; for semiflexible chains we used a bending potential[10] between two consecutive bonds

$$U_b/k_BT = b(1 - \cos\theta)$$

where $\theta$ is a complementary angle to a valence angle and $b$ is a bending parameter introducing the chain stiffness.

For the nonbonded interactions between effective monomeric units, we used a Morse-type potential[9]

$$U_M(r)/\epsilon = \exp[-2\alpha(r - r_{min})] - 2\exp[-2\alpha(r - r_{min})]$$

with parameters $\epsilon/k_BT = 1$ and $\alpha = 24$ and where the minimum of the potential is at $r_{min} = 0.8$. This is a very short-range potential. Interaction diminishes at $r \geq 1$ and the steep wall of the potential for the closest distance of segments is at $\cong$0.76. We will use this value for volumetric properties of the chain. The core volume of the segment/monomeric unit is thus given by a radius $\sigma = 0.76/2$. The choice of interaction strength $\epsilon$ introducing the excluded volume and used in all simulations represents the good solvent condition; the $\Theta$ state is located at $\epsilon/k_BT \approx 1/0.62$.[9] Sampling of conformations to obtain the ensemble averages within the Monte Carlo scheme was performed by chain reptation instead of small random displacement of chain beads which is $N$ times slower in relaxation of chain conformations.

The geometry chosen to represent the confinement by two pores in contact is formed by two interconnected spherical cavities with radii $D_1$ and $D_2$ and with a round connecting aperture of a diameter $W = 4-6$, which is typically smaller than the coil and larger than the chain segment, Figure 1. The size of aperture characterizes interpenetration of cavities and defines also a distance of two cavities. Centers of chain segments are not allowed to move out of this geometry. Since the volumes of cavities defined by the radii above restrict centers of segments the actual wall of each cavity is at a larger radius, $D + \sigma/2$. This correction becomes important for calculating volume properties such as concentration. Volumes of two cavities are defined as partial spherical volumes on two sides of the plane of aperture. This plane divides also chain segments into two cavities in partitioning study. Partition coefficient $K$ is the ratio of concentrations of chain segments in cavities 1 and 2, $K = \phi_1/\phi_2$. The extent of chain confinement is expressed relative to the size of the larger (donor) cavity $D_1$.

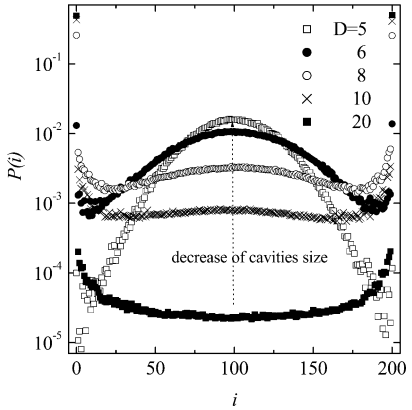


**Figure 2.** Probability of chain conformation having $i$ segments in cavity 1 for the chain length $N = 200$ and the size of cavities indicated in legend.

## Results

First data are collected for unconfined test chains that will be subsequently inserted into the interconnected cavities. A key parameter for partitioning is a confinement, $\lambda = R_g/D$, and we present here the data on radius of gyration $R_g$ of coils in the good solvent ($\epsilon/k_BT = 1$).

Our data for chain lengths in the range of $N = 40-300$ monomer beads (partly shown in Table 1) can be well represented by scaling relations $R_g^2 = 0.0881N^{1.215}$ and $\phi^* = 2.1\,N^{-0.823}$, which have exponents close to the predicted values $^6/_5$ and $-^4/_5$ for good solvent. The concentration of the first coil overlap $\phi^*$ is given as $\phi^* = N(\sigma/R_g)^3$.

**The distribution of the macromolecular chain in a two-cavity volume** is plotted in Figure 2 in terms of normalized probability $P(i)$ of having $i$ segments of total $N = 200$ segments in the cavity 1. $P(i)$, as for other coil properties, is collected as an ensemble average during the simulation. First we investigate the symmetric system with cavity sizes $D_1 = D_2 = 5$, 6, 8, 10, and 20, for $W = 6$ and for flexible chains, $b = 0$. In this case of symmetric distribution of probability the partition coefficient is $K = 1$. This, however, does not mean that distribution of segments between cavities is homogeneous. A strong tendency to occupy only one of the cavities to maximize the conformational entropy of the chain is seen for a weaker confinement. Here, for $D = 8$, 10, and 20, the preferred conformation is the whole coil in either of the two cavities (single cavity conformation). A transition to a bridging conformation (chain located partly in both cavities) appears for the smaller value of $D$ around $D = R_g$ and signaled by increasing probability in the middle range of translocation coordinate $i$. On decrease of $D$, the chain does not fit anymore into a single cavity. Hence for $D = 5$ and 6, the bridging conformation is more favorable. At $D = 6$, the bridging and the coil in single cavity conformations are approximately equally probable. However, we have only two single cavity conformations ($i = 0$ and $i = N$) but a large number of bridging conformations with different numbers of segments in both cavities and with similar probabilities in the middle range of translocation variable $i$.

Respective histograms of the free energy distribution $\Delta A(i)/k_BT$ of conformational states are obtained from the

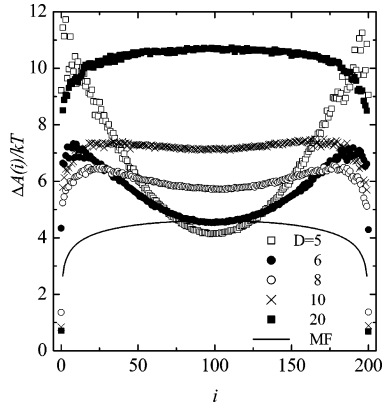


**Figure 3.** Free energy of chain in twin cavity for the states in the previous figure. The solid curve shows a free energy barrier for ideal chain translocation of planar membrane with a hole.

probability $P(i)$ by Boltzmann's law transformation, $\Delta A(i)/k_BT = -\ln P(i)$, for states in Figure 2. We show in Figure 3 that the difference between the bridging and the coil in single cavity conformations is less than $k_BT$ for $D = 6$ (close to the transition) and for other $D$ the differences are up to $(4-10)k_BT$, i.e. strongly in favor of one of two limiting configurations, either the bridging (for smaller $D$) or the single cavity occupation (for larger $D$).

Free energy $\Delta A(i)/k_BT$ for weak confinement in Figure 3 can be compared to translocation across a plane through the hole,[11−13] where chain on both sides of membrane is relatively free. The behavior of chain in cavities for $D = 20$, Figure 3, is very similar in shape to the curve for translocation through a hole with relatively flat distribution over the middle range of translocation variable $i$ and with a strong preference for the single cavity occupancy of chain. From simulation we find a strong dependence of free energy on $i$ for $i$ close to 0 or $N$ (similar to the result of mean-field theory,[11−13] $\Delta A(i)/k_BT \cong 0.5 \ln[i(N - i)]$, for translocation of the ideal chain) as well as a large difference between the two limiting conformations, i.e. bridging and single cavity occupation. The convex curvature in the middle of translocation coordinate seen for weak confinement already ($D = 10$) is in contrast with the concave curvature for the translocation through a hole (or for our results for larger cavities, $D = 20$) and means a slight influence of confinement in both cavities with a beginning of bridging formation. This behavior is amplified for smaller $D$. For strong confinement, a local minimum in $\Delta A(i)$ appears at $i = N/2$. The change of one broad maximum in $\Delta A$ in the middle range of translocation variable $i$ for weak confinement into two local maxima at small and large $i$ for a stronger confinement is observed here for the case of excluded volume chains and increasing confinement. A similar transition was recently described in confined systems with increasing variable excluded volume.[6] Minimum conformation free energy at $i = N/2$ means a stabilization of bridging conformation and leads to a slow down of the translocation process between cavities of comparable size.[6]

Increasing chain rigidity (within the range of semiflexible but still coillike macromolecules) brings about earlier development of bridging conformation for less flexible chains in comparison to flexible chains. This comparison is plotted in Figure 4 for two flexibilities

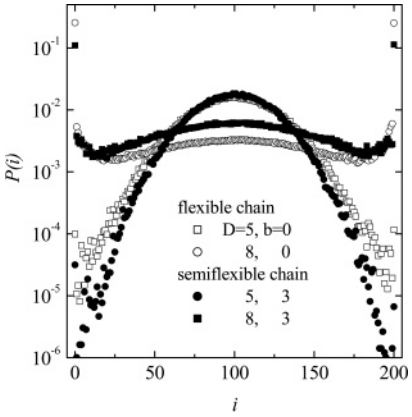


**Figure 4.** Effect of increasing chain rigidity on population of conformations for moderate and strong confinement, $N = 200$.

**Table 1**

| $N$ | $R_g$ | $\phi^*$ |
|---|---|---|
| 50 | 3.19 | 0.0659 |
| 100 | 4.89 | 0.0368 |
| 150 | 6.25 | 0.0263 |
| 200 | 7.41 | 0.0211 |

and for two confinements in the range where bridging of cavities by chain operates. Increase of bridging for stiffer chain can be explained by the increase of coil size respective to that of flexible chain which at a constant volume starts to penetrate partially also the other cavity. Compare the coil size $R_g = 10.02$ for $b = 3$ and $N = 200$ with the smaller value for flexible chain ($b = 0$) in Table 1.

**"Weak" Confinement.** By "weak" confinement we mean here that the effect of crowding (concentration, excluded volume) in two cavities can be neglected. However, in terms of geometrical constraint on the chain in cavities, the confinement can be moderate, affecting considerably the coil conformation. This confinement free energy in a single cavity can be expressed[1] as $\Delta A/kT = -\ln K \cong N D^{-1/\nu}$, ($\nu = 0.588$). From this partitioning into a single confinement one can express also a partitioning of polymer chain between two cavities of different sizes, which is the case to be investigated here

$$K_o = \exp[-(\text{const}) N (D_1^{-1/\nu} - D_2^{-1/\nu})] \qquad (1)$$

We investigate the validity of the above expression separately first as a dependence on $N$ and then on $D_1$, $D_2$. This is because it is common in translocation studies to investigate the dependence of partitioning on $N$. In the first dependence, Figure 5, we plot the free energy $\ln K_o$ vs $N$ for cavities $D_1 = 20$, $D_2 = 10$, and $W = 6$ in the range of chain lengths $N = 1-200$. In this range of weak confinement, where the radii of both cavities are larger than the radius of the largest chain used, we observe a linear dependence as expected. In the second plot, Figure 6, we investigate the partitioning dependence of $\ln K_o$ vs $N(D_1^{-1/\nu} - D_2^{-1/\nu})$ for the constant chain length $N = 100$ and cavities in the range of $D_1 = 10-20$ and $D_2 = 6-10$ with constant aperture $W = 6$. This results into a broad extent of partitioning between two cavities in the range of $K_o = 1-42$. Since this is also a "weak" confinement we observe dependence according to eq 1. A master plot of all data from both plots in Figures 5 and 6 can be constructed (not shown) where all data form a master plot (except 2−3 points for largest

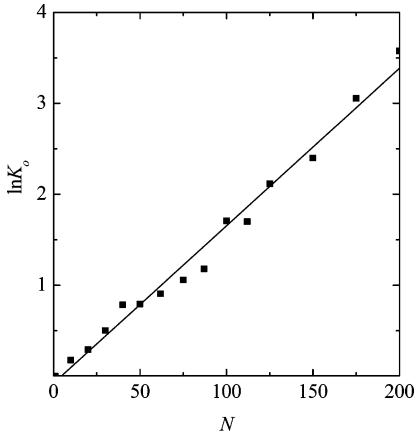


**Figure 5.** Partitioning free energy ln $K_o$ vs $N$ for cavities $D_1 = 20$, $D_2 = 10$, $W = 6$, and the range of chain lengths $N = 1-200$.

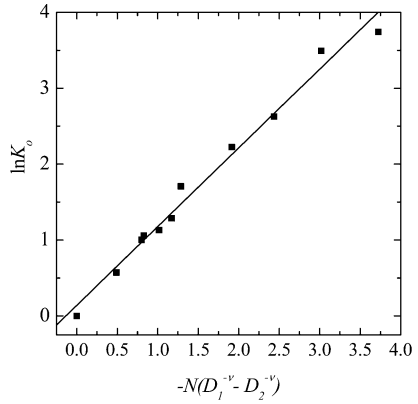


**Figure 6.** Partitioning free energy ln $K_o$ vs $N(D_1^{-1/\nu} - D_2^{-1/\nu})$ for the constant chain length $N = 100$ and cavities in the range of $D_1 = 10-20$ and $D_2 = 6-10$.

values of ln $K_o$ in both dependences)according to eq 1 with const = 1.215.

**Strong Confinement with Intervention of Crowding.** At stronger confinement the partitioning behavior between two cavities starts to deviate from eq 1. On increase of $N$, the initial increase seen in plot of ln $K$ vs $N$ is followed by a maximum and then a decrease, Figure 7. The maximum was explained by presence of excluded volume, or crowding of segments.[4-6] Since this is a single chain problem the term concentration was avoided. However, if the chain length of a macromolecule is increased within the system of two small cavities actually the concentration increases also; hence, we introduce here the concentration dependence of $K$ directly even if we are concerned with a single chain. The effect of concentration can be neglected in the above example of weak confinement. However, as is known for the partitioning from bulk polymer solution to pores the increasing concentration in bulk solution drives chains into pores and concentration in different pores start to equalize.[7] For stronger confinement thus one expects decrease of ln $K$ on increasing $N$ instead of an increase as for the weak confinement. Similar behavior was observed earlier in partitioning in interconnected cavities on increase of excluded volume in confined chains.[4-6] Here this example is illustrated by simulation data for $D_1 = 6$, $D_2 = 4$, $W = 4$ and a range of excluded volume chain lengths $N = 10-200$ shown in Figure 7.

Decomposition of the free energy of a macromolecule in cavities into a confinement and a concentration effect

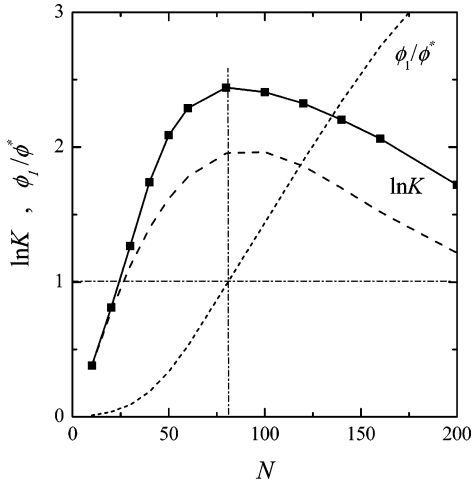


**Figure 7.** Partitioning free energy (solid curve with squares are MC data, dashed curve is the result of eq 1−3) and corresponding reduced concentration in the larger cavity as a function of chain length of encased macromolecule, $N = 10-200$ and $D_1 = 6$, $D_2 = 4$, $W = 4$.

proves to be useful here in a similar way as used for the partitioning of macromolecules between bulk solution and a slit confinement.[14] At equilibrium the chemical potential in cavity 1 and 2 are equal.

$$\Delta\mu_1(\phi_1) = \Delta\mu_2(\phi_2) + kT \ln K_o \qquad (2)$$

The free energy of macromolecule is affected by confinement in each cavity and the second term on the rhs collects this influence in both cavities into a difference in confinement free energy as given by eq 1. Each of two concentration dependent chemical potentials $\Delta\mu_j$ of the polymer is approximated by the expression of Flory, used here for the condition of good solvent by omitting the interaction term.

$$\Delta\mu_j/k_BT = \ln \phi_j + (1 - \phi_j)(1 - M) \quad \text{for cavities } j = 1, 2 \quad (3)$$

$$\text{for } \; j = 1, \;\; M = i$$

$$\text{for } \; j = 2, \; M = N - i$$

For shorter chains in the twin cavity (or larger cavities equivalently), which represent a dilute solution, the chemical potential in eq 2 is well approximated by the first ideal term in eq 3. In this case eq 2 reduces to eq 1 and the free energy is given by relation[1] linear in $N$, given solely by confinement difference in the two cavities. This behavior is seen in Figure 7 for $N < 50$.

To account for the whole concentration range we use the approximate separation of confinement and concentration effects as given by eq 2 and 3 and we approximate the confinement term in eq 2 by ln $K_o = 0.0446N - 0.0609$ (according to eq 1), which is obtained from the linear fit of initial part ($N < 50$) of ln $K$ vs $N$ plot, Figure 7. It should be reminded here that the original relation, eq 1, was derived for the strong confinement and thus its validity for stronger confinement, represented here by longer chains in given cavity, is expected. Equation 2 is solved numerically. In contrast to partitioning of macromolecules from bulk solution to a single cavity, where the bulk solution serves as a reservoir of chains, none of two concentrations in two cavities here can be chosen initially. Equilibrium concentrations in two cavities are established according

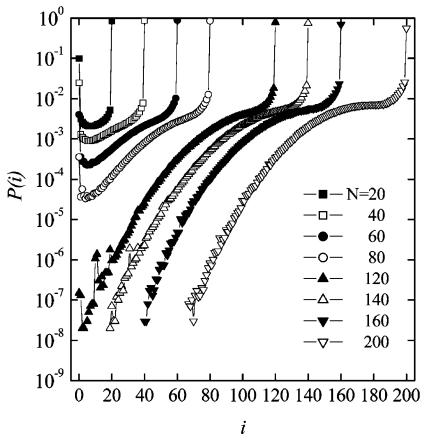


**Figure 8.** Probability of conformations for the states defined in Figure 7 along the increase of conformer population from the single cavity occupation to the bridging conformation.

to the system of eqs 1−3 by the chain length $N$ and two confinements as parameters. Hence, in addition a mass balance in cavities, $NV_{ch} = V_1\phi_1 + V_2\phi_2$, has to be taken into account ($V_{ch}$, $V_1$, $V_2$ are volumes of the chain and the cavities 1 and 2). Volume of the chain $V_{ch}$ is approximated in this system with continuous interaction potential by the volume $Nl\pi(\sigma/2)^2$ of a cylinder of $N$ bonds of length $l$ and radius $\sigma$. Resulting equilibrium concentrations in two cavities define the partition coefficient at nondilute solution, $K = \phi_1/\phi_2$. $K$ is different from the ratio of number of chain segments in each cavity or at each side of membrane (as sometimes used in translocation) by a constant given by the ratio of cavity volumes.

The maximum in the free energy vs $N$ from simulation results as seen from Figure 7 is reproduced by the scheme of eq 1−3 about at the same position. The trend for all chain lengths used is similar as well. In the same figure, we plot also the reduced concentration in the larger cavity. From the comparison of two curves it is clear that for concentrations in larger cavity lower than the coil overlap concentration, $\phi_1/\phi^* = 1$, the equilibrium follows closely eq 1. About at "overlap" concentration (the coil just fits into a larger cavity), the maximum appears, and at higher concentrations (stronger confinement/longer chain), the preference of the chain for the larger cavity starts to disappear with more extensive penetration of chain segments also into the smaller cavity. The approach based on eq 1−3 is a simple approximation based on homogeneity of concentration in cavities and model separation of confinement and concentration. Nevertheless, it is clear that this simple approach becomes useful concept for fully encased chains at stronger confinement where the effect of concentration cannot be neglected.

Histograms of chain distribution for the above case with maximum in ln $K$ vs $N$, Figure 7, show further details on the extent of chain propagation over two cavities. From Figure 8, it is seen that a strong preference for the whole chain to stay in one of the cavities is similar to the symmetric distribution shown in Figure 2. Of course, in this asymmetric case, the preference is much stronger for the larger cavity and on increasing $N$ is deepened. Shape of the probability distribution for weak confinement corresponds to that shown for the free energy of translocation through a membrane[11,13] for both symmetric (seen in Figure 3 for $D = 20$) and asymmetric ($N < 60$ here) cases: a strong preference for the nonbridging conformation (the whole coil is in cavity 1 or 2) and a proportional development between these two cases. In our case the difference at two sides of aperture is given by a difference in confinements in two cavities, $D_1 \neq D_2$, instead of a general difference in chemical potential between the two sides of membrane with a hole. Bridging conformations are marginal for shorter chains, $N < 60$. It was observed before that the maximum corresponds to the size of the coil approximately equal to the size of the larger cavity.[15] From our results we see that the loss of linearity and the maximum appears already for smaller coils. At stronger confinements ($N > 60$), the bridging conformations start to be populated considerably and this is effective over and after the maximum, already at the decrease of ln $K$ in Figure 7. A correspondence between histograms of conformational probability $P(i)$ and partition coefficient $K$ is expected since from the histogram we can obtain the equilibrium number of segments $\bar{n}_1$ in cavity 1 and from this also $K$.

$$\bar{n}_1 = \sum_{i=1}^{i=N} iP(i),\ K = \frac{\bar{n}_1}{N - \bar{n}_1}\frac{V_2}{V_1} \tag{4}$$

The bridging conformation is seen in increasing probability in the middle range of translocation coordinate $i$. This is a characteristic difference between the translocation through a hole (where chains are less confined at both sides of a membrane) and the translocation between two cavities with stronger confinement. The behavior of histograms respects the position of maximum in Figure 7. As seen for longer chains, $N \geq 60$, the change of curvature in the middle of distribution relative to shorter chains represents the increase of population of bridging conformation in the twin cavity due to the crowding effect.

**Chain Structure in Cavities.** To assess the structure of chains in the twin-cavity volume we estimated also the single chain structure factor defined for isotropic system as

$$S(q) = \frac{1}{N^2}\sum_{i=1}^{N}\sum_{j=1}^{N}\sin(qr_{ij})/qr_{ij} \tag{5}$$

for three typical situations defined by the extent of confinement. We used the wavenumber $q = 2\pi/x$ in the range from macroscopic size $x$ to about a monomer size $x$; the largest $q$ used ($q = 4$) represents approximately the smallest distance $x$ of about two bond lengths. The log−log plots of $S(q)$ vs $q$ are depicted in Figure 9. Inserted lines next to the curves represent the slope of theoretical scaling exponents in the Kratky regime for the respective states described below.

The first example is for a weak confinement $D_1 = 20$, $D_2 = 10$, and $N = 175$. Here the chain, though confined, behaves as a free excluded volume chain with the structure factor scaling as for the good solvent chain, $S(q) \sim q^{-1.7}$. The second example represents a moderate confinement, $D_1 = 6$, $D_2 = 4$, and $N = 80$, which is the state about at maximum in Figure 7. Here the coil is more compact than the free coil in good solvent; it feels the confinement and resembles the coil of Θ or ideal chain with the corresponding scaling $S(q) \sim q^{-2}$. The third example represents a strong confinement and is the structure of the longest confined chain in Figure 7, $D_1 = 6$, $D_2 = 4$, $N = 200$. This coil is a strongly squeezed chain in spherical confinement and resembles the

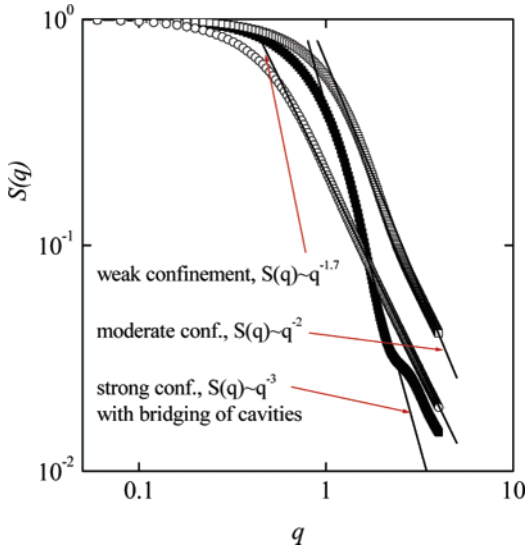


**Figure 9.** Typical structure factors for coils in interconnected cavities for weak, moderate and strong confinement. Parameters for these systems are listed in the text.

polymer globule on a larger scale, $S(q) \sim q^{-3}$. In addition, this structure factor shows a break reflecting the presence of chain in two different cavities. The $q$-position of the break represents approximately the size of smaller cavity or of the size of aperture.

## Conclusions

Partitioning of macromolecules into micropores was recently newly pioneered by a molecular experiment with visualization of single DNA macromolecules encased in two interconnected cavities. A molecular simulation of the excluded volume chain in this situation was performed here and was focused on the distribution of conformations in the twin cavity and on the conformation transition appearing on the increase of confinement from single cavity occupation to the conformation bridging two cavities. We show data for the existing theory or its further development and present a simple concept of interplay of confinement and concentration for macromolecules encased in the interconnected cavities.

Our simulation of excluded volume macromolecule encased in two interconnected cavities reveal for broader cavities a strong preference for the nonbridging conformation observed from histograms of conformation free energy.

For the case of the symmetric twin-cavity system a conformation transition from single cavity occupation to the conformation with bridging of two cavities is observed on increasing confinement of encased chain. This is signaled by transition of one broad maximum of free energy in the midpoint of translocation into two local maxima close to the weak and the full translocation.

In the case of asymmetric system the partitioning of chain between two cavities is governed by classical partitioning law for weak confinement, ln $K_o$ is linear with $N(D_1^{-1/\nu} - D_2^{-1/\nu})$. For longer chains (stronger confinement) a maximum followed by a decrease is explained by a simple model of interplay between increasing confinement and increasing concentration for encased chain. The position of the maximum reflects increasing hindrance of the macromolecule in the larger cavity and the start of the population of a bridging conformation, which is also observed from the histogram of conformations.

The structure of coils in the twin cavity is reflected by typical structure factors $S(q)$ of the free expanded coil for the weak confinement, about the $\Theta$ coil for the moderate confinement and the polymer globule with a break in $S(q)$ (appearing from the structure of twin cavity) for strongly confined macromolecular chain.

**Acknowledgment.** This work was supported partially by Science and Technology Assistance Agency under the contract No. APVT-51-044902 and VEGA 2/3013/23.

## References and Notes

(1) Daoud, M.; de Gennes, P. G. *J. Phys. (Paris)* **1997**, *38*, 85−93.
(2) Bustamante, J. O.; Hanover, J. A.; Liepins, A. *J. Membr. Biol.* **1995**, *146*, 239−251.
(3) Nykypanchuk, D.; Strey, H. H.; Hoagland, D. A. *Macromolecules* **2005**, *38*, 145−150.
(4) Tsonchev, S.; Coalson, R. D. *Chem. Phys. Lett.* **2000**, *327*, 238−244.
(5) Chern, S.-S.; Coalson, R. D. *J. Chem. Phys.* **1999**, *111*, 1778−1781.
(6) Kong, C. K.; Muthukumar, M. *J. Chem. Phys.* **2004**, *120*, 3460−3466.
(7) Cifra, P.; Bleha, T.; Wang, Y.; Teraoka, I. *J. Chem. Phys.* **2000**, *113*, 8313−8318.
(8) Muthukumar, M. *Phys. Rev. Lett.* **2001**, *86*, 3188−3191. Loebl, H. C.; Randel, R.; Goodwin, S. P.; Matthai, C. C. *Phys. Rev.* **2003**, *E67*, 041913-(1−5). Muthukumar, M. *J. Chem. Phys.* **2003**, *118*, 5174−5184. Randel, R.; Loebl, H. C.; Matthai, C. C. *Macromol. Theory Simul.* **2004**, *13*, 387−391. Matsuyama, A. *J. Chem. Phys.* **2004**, *121*, 8098−8103. Kirmizialtin, S.; Ganesan, V.; Makarov, D. E. *J. Chem. Phys.* **2004**, *121*, 10268−10277.
(9) Pandey, R. B.; Milchev, A.; Binder, K. *Macromolecules* **1997**, *30*, 1194−1204.
(10) Fynewever, H.; Yethiraj, A. *J. Chem. Phys.* **1998**, *108*, 1636−1644.
(11) Sung, W.; Park, P. J. *Phys. Rev. Lett.*, **1996**, *77*, 783−786.
(12) DiMarzio, E. A.; Mandell, A. J. *J. Chem. Phys.* **1997**, *107*, 5510−5514.
(13) Muthukumar, M. *J. Chem. Phys.* **1999**, *111*, 10371−10374.
(14) Škrinárová, Z.; Bleha, T.; Cifra, P. *Macromolecules* **2002**, *35*, 8896−8905.
(15) Tsonchev, S.; Coalson, R. D.; Chern, S.-S.; Duncan, A. *J. Chem. Phys.* **2000**, *1113*, 8381−8389.

MA050147G